



**HAL**  
open science

## Microglia mitigate neuronal activation in a zebrafish model of Dravet syndrome

Alexandre Brenet, Julie Somkhit, Zsolt Csaba, Sorana Ciura, Edor Kabashi, Constantin Yanicostas, Nadia Soussi-Yanicostas

► **To cite this version:**

Alexandre Brenet, Julie Somkhit, Zsolt Csaba, Sorana Ciura, Edor Kabashi, et al.. Microglia mitigate neuronal activation in a zebrafish model of Dravet syndrome. 2022. hal-03745018v2

**HAL Id: hal-03745018**

**<https://hal.science/hal-03745018v2>**

Preprint submitted on 5 Aug 2022 (v2), last revised 22 Oct 2022 (v3)

**HAL** is a multi-disciplinary open access archive for the deposit and dissemination of scientific research documents, whether they are published or not. The documents may come from teaching and research institutions in France or abroad, or from public or private research centers.

L'archive ouverte pluridisciplinaire **HAL**, est destinée au dépôt et à la diffusion de documents scientifiques de niveau recherche, publiés ou non, émanant des établissements d'enseignement et de recherche français ou étrangers, des laboratoires publics ou privés.

# Microglia mitigate neuron excitation in a zebrafish model of Dravet syndrome

Alexandre Brenet<sup>1</sup>, Julie Somkhit<sup>1</sup>, Constantin Yanicostas<sup>1</sup>, and Nadia Soussi-Yanicostas<sup>1\*</sup>

<sup>1</sup>NeuroDiderot, Inserm U1141, Université Paris Cité, Hôpital Robert Debré, Paris, France.

#Corresponding Author:

Dr. Nadia Soussi-Yanicostas  
Hôpital Robert Debré, INSERM  
48, Bd Sérurier  
75019 Paris France,  
Tel: +33-1 40 03 19 31  
E-mail: [nadia.soussi@inserm.fr](mailto:nadia.soussi@inserm.fr)

**Keywords:** Microglia, Epilepsy, Seizure, Calcium imaging, Zebrafish, Seizures, Cytokines, Neuroprotection

**Running title:** microglia remodelling in epilepsy

## **Abstract**

It is long known that epileptic seizures induce brain neuroinflammation through the activation of microglia, but these cells have not yet received the attention they deserve in epilepsy research. In particular, the consequences of this microglial response on subsequent neuron excitability remain poorly understood. Here, we sought to fill this gap and gain a fuller understanding of the role of microglia in the pathophysiology of epilepsy, using an established zebrafish Dravet syndrome epilepsy model based on *Scn1Lab* sodium channel loss-of-function, combined with live microglia and neuronal  $Ca^{2+}$  imaging, local field potential (LFP) recording and genetic microglia ablation. First, in *scn1Lab*-deficient embryos experiencing epileptiform seizures, microglia displayed morphological and biochemical features suggesting M1-like proinflammatory activation including reduced branching and amoeboid-like morphology, combined with a marked increase in the number of microglia expressing pro-inflammatory cytokine  $Il1\beta$ . More importantly, *scn1Lab*-KD embryos fully lacking microglia showed a significantly increased neuronal excitation compared to that seen in *scn1Lab*-KD individuals with microglia, as shown by LFP recording and  $Ca^{2+}$  imaging, and also by the epileptiform seizure-related whirling swimming of larvae. Taken together, these findings are evidence that notwithstanding microglia activation and the synthesis of proinflammatory cytokines, microglia provide neuroprotection to epileptic neuron networks, making these cells a promising therapeutic target in epilepsy.

## Introduction

Epilepsy is the most frequent neurological disorder, affecting more than 1% of the world's population (Fisher *et al.*, 2014) (Fisher, 2015). The disease is characterized by recurrent seizures caused by synchronized hyperexcitation of neuronal networks of various sizes ranging from a limited brain region to the whole cortex, leading to focal or generalized seizures, respectively (Thurman *et al.*, 2011), (Carmant, 2015), (World Health Organization, 2019). Potent anti-epileptic drugs (AEDs) have been developed over the last decades. However, they are ineffective in approximately one third of patients, especially children with developmental epileptic encephalopathies, such as Dravet syndrome (DS) (Brunklau, Dorris and Zuberi, 2011; Wu *et al.*, 2015) (Kwan, Schachter and Brodie, 2011). In addition, they can cause very severe side effects, such as teratogenicity in pregnant women (Marxer *et al.*, 2021), (Xue-Ping *et al.*, 2019). These limitations emphasize the need for novel anti-epileptic strategies. It is noteworthy that most existing AEDs are “neurocentric”, targeting neuronal proteins directly involved in neuronal network excitation, while microglia have so far received little attention as a therapeutic target in epilepsy. This is despite large amounts of data accumulated over the last decades strongly suggesting that these cells are important players in the pathophysiology of the disease (Vezzani, Balosso and Ravizza, 2019).

Microglial cells, the resident brain macrophages, have several essential functions, including immunoprotection, maintenance of neuron health and homeostasis, and maturation of neuronal networks through developmentally controlled apoptosis of supernumerary neurons and pruning of excess synapses (Lukens and Eyo, 2022). As immune cells, microglia also respond rapidly to brain injury or infection through complex reprogramming, referred to as microglia activation, which comprises morphological and biochemical changes, including the synthesis and release of pro-inflammatory cytokines (Woodburn, Bollinger and Wohleb, 2021). In epileptic patients, it has long been known that seizures cause the activation of microglial cell and synthesis of inflammatory mediators (Vezzani, Balosso and Ravizza, 2019b), (Ravizza *et al.*, 2008), (Vezzani, 2013) (Vezzani *et al.*, 2008), and the analysis of post-mortem brain tissues from epileptic patients has shown massive microglia activation, directly correlated with seizure severity (Boer *et al.*, 2008), (Morin-Brureau *et al.*, 2018). Moreover, in various pharmacological rodent epilepsy models, pronounced morphological changes of microglia were rapidly observed after seizures, prior to the onset of neuron damage (Eyo *et al.*, 2014), (Avignone *et al.*, 2015). However, other studies have highlighted the wide variability of inflammatory responses seen in both human patients and animal epilepsy models (Gasmi *et al.*, 2021). Some data suggest that microglia may be harmful in an epileptic context, probably owing to the release of pro-inflammatory cytokines, known to be pro-epileptogenic factors (Vezzani *et al.*, 1999) (Andoh, Ikegaya and Koyama, 2019) (Rana and Musto, 2018). Conversely, other

studies suggest that microglia may play a beneficial role in epilepsy by decreasing the excitability of neuronal networks (Badimon *et al.*, 2020) (Eyo *et al.*, 2014) (Li, X. Du, *et al.*, 2012) (Vinet *et al.*, 2012). Data also suggest that the response of microglia to epileptic seizures is not uniform throughout the brain with cells showing a wide range of phenotypes within the same individual (Morin-Brureau *et al.*, 2018). Moreover, the levels of both pro-inflammatory and anti-inflammatory cytokines are increased in microglia after epileptic seizures, supporting the notion that the response of these cells to seizures is not limited to classic M1-type pro-inflammatory activation, thus highlighting the complexity of this microglial response (Benson *et al.*, *Epilepsia* 2015, 56, 895–905). Thus, whether microglia activity has an overall detrimental or beneficial role in epilepsy is thus still a largely open question with far-reaching therapeutic implications (Lukens and Eyo, 2022).

To address this issue and gain a better understanding of the role of microglia in epilepsy, we used a zebrafish model of Dravet syndrome (DS), a severe intractable epileptic syndrome in infants caused in 70–80% of cases by *de novo* mutations in the gene encoding the voltage-gated sodium channel, *SCN1A* (Dravet, 2011) (Claes *et al.*, 2001). We used this zebrafish epilepsy model to investigate the morphology and dynamic behaviour of microglial cells *in vivo*, using the Tg[mpeg1:mCherryF], which allows imaging of microglial cells in living zebrafish embryos and larvae combined with neuronal Ca<sup>2+</sup> imaging, local field potential (LFP) recording and genetic microglia ablation.

We found that microglia were deeply remodelled in *scn1lab*-deficient larvae, with morphology shifted toward the amoeboid and less branched phenotype, combined with a markedly increased mobility of their cell bodies and an increased number of I11 $\beta$ -expressing cells. In addition, in microglia-depleted *scn1lab*-deficient larvae, neuronal hyperexcitation was significantly increased compared with their siblings with microglia, suggesting that activities of these cells lent neuroprotection to epileptic neurons and decreased their excitability.

## Results

### Microglia morphological changes in *scn1Lab*-KD embryos

To gain a fuller understanding of microglia phenotypes in epileptic brains *in vivo*, we first made use of the live imaging techniques available in zebrafish (Hassan-Abdi *et al.*, 2019), combined with two zebrafish *scn1Lab* models of Dravet syndrome epilepsy (Baraban, Dinday and Hortopan, 2013a) (Brenet *et al.*, 2019), and real-time microglia imaging. We used 4 days post-fertilization (dpf) *scn1Lab* morphant and *scn1Lab*<sup>s552/s552</sup> mutant embryos, which both show recurrent spontaneous epileptiform seizures, as visualized by LFP recording and Ca<sup>2+</sup> imaging, and by the characteristic swirling behaviour of the larvae (Baraban, Dinday and Hortopan, 2013b) (Zhang *et al.*, 2015) (Brenet *et al.*, 2019). Specifically, we mainly used *scn1Lab* morphants, referred to below as *scn1Lab*-KD individuals, and verified that the results were identical in *scn1Lab*<sup>s552/s552</sup> mutants, displaying full loss of Scn1Lab function (Baraban, Dinday and Hortopan, 2013b) (Brenet *et al.*, 2019). To visualize microglial cells *in vivo*, we chose the transgenic Tg[*mpeg1*:mcherryF] line, which shows intense labelling of these cells (Travnickova *et al.*, 2015). However, because this transgenic is expressed in both microglia and macrophages, we verified that all the microglia imaged in this study also expressed the Tg[*p2y12*:GFP] transgene, which is specifically expressed in these cells (Mildner, 2017). As previously shown (Peri and Nüsslein-Volhard, 2008a) (Hassan-Abdi *et al.*, 2019), in WT larvae, microglia displayed the characteristic ramified morphology of "resting" microglia, with a relatively small cell body and several elongated and ramified branches (**Figure 1A**; **1A1-3 and Supp. Fig. 1A<sub>2</sub> (Video 1)**: <https://urlz.fr/iPxZ>). By contrast, in *scn1Lab*-KD larvae, microglia exhibited a more rounded morphology, with a larger cell body combined with fewer and shorter branches (**Figure 1B**; **1B1-3 and Supp. Fig. 1B<sub>3</sub> (Video 2)**: <https://urlz.fr/iPxP>). To further characterize the morphological differences in the two genetic contexts, we used the 3D image analysis software Imaris to measure several microglial cell morphological parameters (sphericity, volume, surface area, branch number, branch length and ramification index) (Bitplane). Data confirmed that microglia in *scn1Lab*-KD larvae displayed an increased sphericity (WT: 0.567 ± 0.006 vs *scn1Lab*: 0.644 ± 0.006; *p* < 0.0001) (**Figure 1C**), a decreased number of branches (WT: 6.3 ± 0.2 vs *scn1Lab*: 5.1 ± 0.2; *p* < 0.0001) (**Figure 1D**), a decreased total (WT: 115 ± 3 µm vs *scn1Lab*: 85 ± 3 µm; *p* < 0.0001) (**Figure 1E**) and mean branch length (control: 23.5 ± 0.4 µm vs *scn1Lab*: 19.6 ± 0.3 µm; *p* < 0.0001) (**Figure 1F**), and a decreased ramification index (WT: 1.94 ± 0.05 vs *scn1Lab*: 1.74 ± 0.05; *p* < 0.0001) (**Figure 1G**) compared with microglia in WT individuals. Sholl analysis, a method used to quantify both the extent and complexity of cell branches (Fiji software), further confirmed that microglia in *scn1Lab*-KD individuals had fewer and shorter branches than their WT siblings (**Figure 1H**).

Taken together, our data show that microglia exhibited an amoeboid-like morphology reminiscent of that of M1-type activated macrophages in *scn1Lab*-KD larvae.

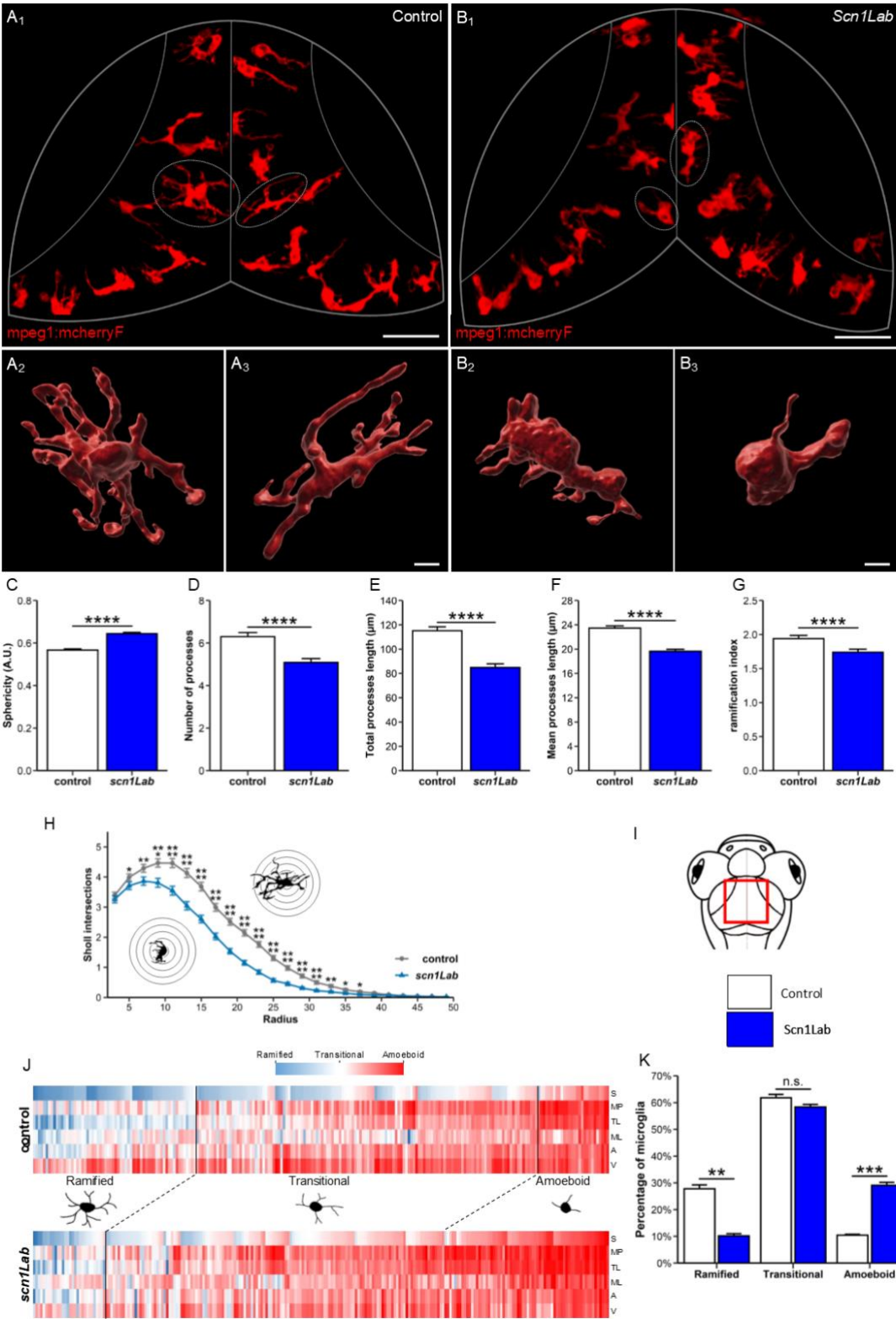


**Figure 1: Microglial morphology in the *scn1Lab* model.**

(A-B) Dorsal view of 4 dpf Tg[mpeg1:mcherryF] control (A) and *scn1Lab* (B) larvae optic tectum showing microglial cell population. (C-D) 3D reconstruction of control (C) and *scn1lab* (D) microglia.. (E-I) Quantification of microglial cells' sphericity (E), number of processes (F), total processes length (G), mean processes length (H) and ramification index (I) in 4 dpf *scn1Lab* larvae ( $N = 11$ ;  $n = 239$ ) compared to sibling controls ( $N = 11$ ;  $n = 228$ ). (H) Sholl analysis of control (grey) and *scn1Lab* (blue) microglia. (I) Diagram of the head of a zebrafish larva with the area of interest (the periventricular stratum) framed in red. (J) Cluster analysis of the microglial population of 4 dpf *scn1Lab* ( $N = 11$ ;  $n = 239$ ) and sibling control ( $N = 11$ ;  $n = 228$ ) based on sphericity (S), number of microglial processes (MP), total processes length (TL), mean processes length (ML), area (A) and volume (V), leading to three microglial populations. (K) Repartition of the control (white) and *scn1lab* (blue) microglial population in the three clusters produced before. All images were acquired with SP8 Leica scanning laser confocal equipped with 20x/multi-immersion 0.75 objective. All data are represented as the mean  $\pm$  sem.  $p$ -values were determined using Mann Whitney or unpaired Student  $t$ -test depending on the normal distribution of the values. n.s., non-significant; \*\*,  $p < 0.01$ ; \*\*\*,  $p < 0.001$ ; \*\*\*\*,  $p < 0.0001$ . Scale bars=50  $\mu$ m (A,B).; 10  $\mu$ m (A<sub>2</sub>, A<sub>3</sub>, B<sub>2</sub>, B<sub>3</sub>).

To better evaluate the extent of microglia morphological differences in *scn1Lab*-KD and WT larvae, we performed a cluster analysis of these cells in the two genetic contexts, based on the five morphological parameters showing significant changes as indicated above (sphericity, branch number, branch length, surface area, and volume) (see Materials and Methods). The first population comprised cells showing low sphericity, numerous elongated branches, and high surface area and volume: these are referred to below as "branched" microglia. The second comprised microglia displaying high sphericity, few short processes, and low surface area and volume, referred to below as "amoeboid" cells. The third comprised cells with intermediate characteristics, referred to below as "transitional" microglia (**Figure 1J**). Although the three populations of microglia were found in both contexts, their respective proportions varied considerably. In *scn1Lab*-KD larvae, we observed a significant increase in the percentage of "amoeboid" microglia ( $29.1 \pm 1.2$  vs  $10.4 \pm 0.3\%$ ;  $p < 0.001$ ) combined with a significant decrease in the percentage of "branched" microglia ( $10.2 \pm 0.8$  vs  $27.8 \pm 1.5\%$ ;  $p < 0.01$ ) (**Figure 1K**). These findings are further evidence that microglia display an M1-like reactive phenotype in *scn1Lab*-KD larvae.

Visual examination of the behaviour of microglia in *scn1Lab*-KD and WT larvae provided a first indication that these cells displayed an increased mobility in the mutant context. To confirm this observation, we measured the movement speed of microglia cell bodies in the two genetic contexts. In WT embryos, as previously described (Hassan-Abdi *et al.*, 2019), microglia had several branches that were constantly extending and retracting, while their cell bodies



remained almost immobile (**Figure 2A<sub>1</sub>-A<sub>2</sub>, 2C<sub>1</sub>, 2F<sub>1</sub>**) (**Supp. Video 3**, <https://urlz.fr/iOlz>). By contrast, cell bodies of *scn1Lab*-KD microglia were much more mobile (**Figure 2B<sub>1</sub>-B<sub>2</sub>, 2C<sub>2</sub>, 2F<sub>2</sub>**) (**Supp. Video 4**, <https://urlz.fr/iOIA>).

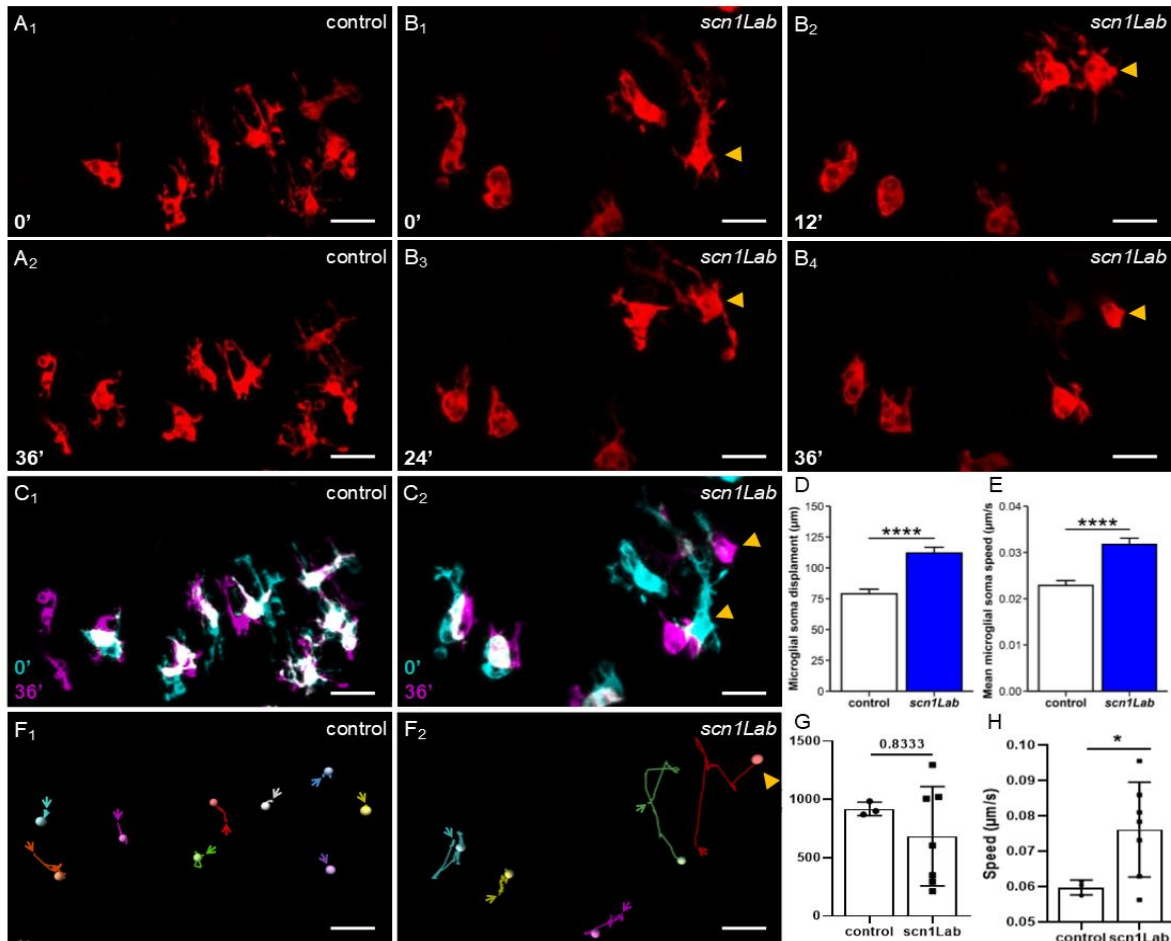


**Figure 2: Microglial dynamic in the *scn1Lab* model.**

**(A)** Confocal time-lapse showing microglial dynamic in a 4 dpf Tg[mpeg1:mcherryF] control living larval brain. **(B)** Confocal time-lapse showing microglial dynamic in a 4 dpf Tg[mpeg1:mcherryF] *scn1Lab* living larval brain. **(C)** Merged image of two time points (0' in red 60' in green) highlighting the increase in microglial soma displacement in *scn1Lab* larvae (**C<sub>2</sub>**) compared to sibling control (**C<sub>1</sub>**) (cyan = 0', magenta = 36', white = merge). **(D)** Quantification of microglial cell body speed displacement over 36' recording in 4 dpf *scn1Lab* larvae ( $N = 6$ ;  $n = 55$ ) compared to sibling controls ( $N = 4$ ;  $n = 46$ ). **(E)** Quantification of microglial cell body mean speed 60' recording in 4 dpf *scn1Lab* larvae ( $N = 6$ ;  $n = 55$ ) compared to sibling controls ( $N = 4$ ;  $n = 46$ ). **(F)** Microglial cell tracking over 60' in 4 dpf control (**F<sub>1</sub>**) and *scn1Lab* (**F<sub>2</sub>**) living larval brain. **(G)** Quantification of microglial processes displacement over 60' recording in 4 dpf *scn1Lab* larvae ( $N = 1$ ;  $n = 7$ ) compared to sibling controls ( $N = 1$ ;  $n = 3$ ). **(H)** Quantification of microglial processes speed over 60' recording in 4 dpf *scn1Lab* larvae

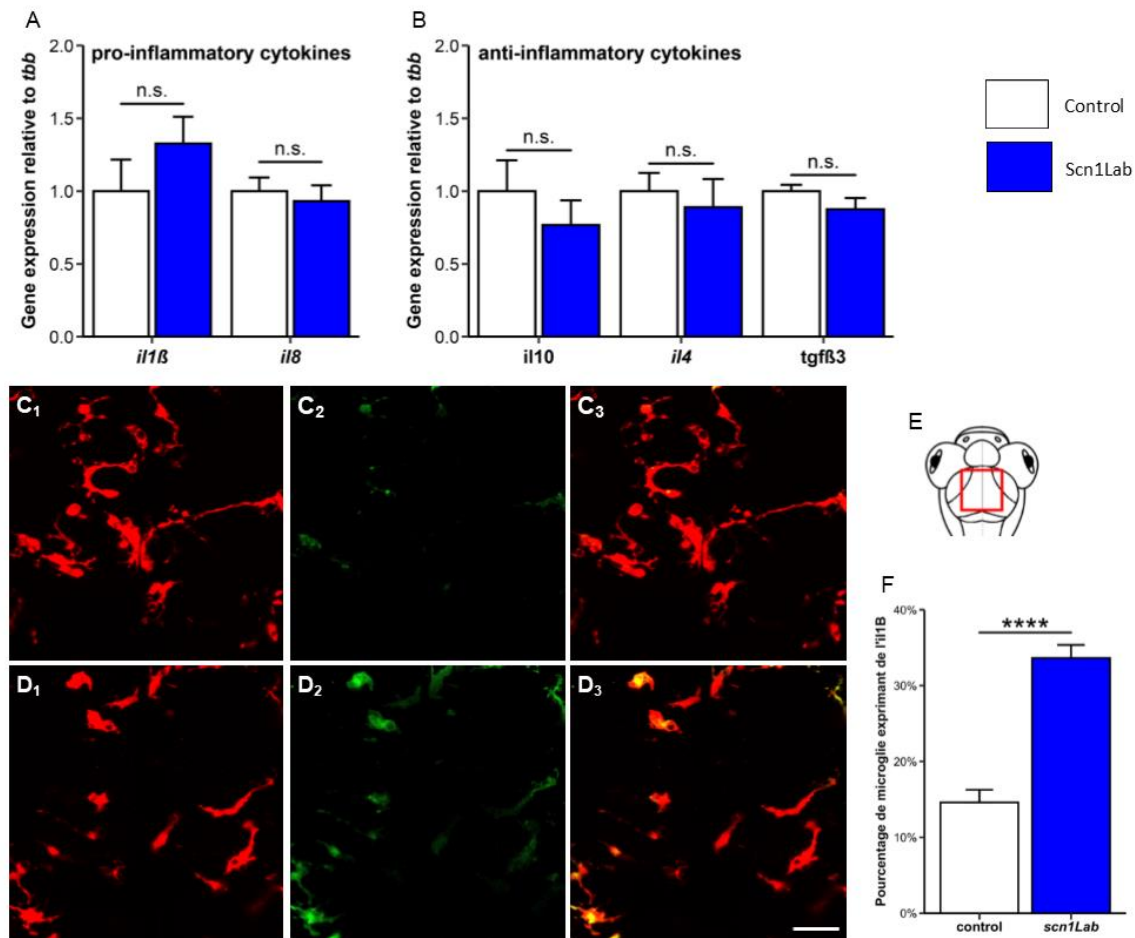
( $N = 1$ ;  $n = 7$ ) compared to sibling controls ( $N = 1$ ;  $n = 3$ ). Scale bar 20  $\mu\text{m}$  in all images.  $N =$  number of larvae and  $n =$  number of microglial cells. All images were acquired with a SP8 Leica laser scanning confocal equipped with a 40x/water 1.1 objective. All data are represented as the mean  $\pm$  sem.  $p$ -values were determined using Mann Whitney test. \*\*\*\*,  $p < 0.0001$ .

*The time-lapse sequences of microglia dynamics in  $Tg(mpeg1:mcherry; scn1lab-KD)$  brain showed the rapid changes of morphology of these cells (Figure 1B<sub>1</sub>- B<sub>4</sub>, yellow arrowhead). The merged sequence images at  $t = 0$  minutes (blue) and  $t = 36$  minutes (pink) highlighted the increased mobility of microglial cell bodies in the  $scn1Lab$  model (Figure 2C<sub>2</sub>) compared with the control (Figure 2C<sub>1</sub>). We next tracked WT (Figure 2F<sub>1</sub> and Supp. Video 5. <https://urlz.fr/iOIG>) and  $scn1Lab-KD$  (Figure 2F<sub>2</sub> and Supp. Video 6. <https://urlz.fr/iOIG>) microglia and measured the distance travelled by these cells (Figure 2F<sub>1</sub>-F<sub>2</sub>). Results show microglia travelled a greater distance in  $scn1Lab-KD$  larvae than in WT larvae ( $112.0 \pm 4.7$  vs  $78.9 \pm 3.8 \mu\text{m}$   $p < 0.0001$ ) (Figure 2D). Microglia therefore moved faster in  $scn1Lab-KD$  larvae than in WT ( $0.0317 \pm 0.0014$  vs  $0.0229 \pm 0.0011 \mu\text{m/s}$ ;  $p < 0.0001$ ) than those in WT (Figure 2E).*

### **Increased microglia-mediated brain inflammation in $scn1Lab-KD$ embryos**

Because the microglia phenotypic changes observed in  $scn1Lab-KD$  larvae were strongly reminiscent of those of "activated" M1-type neuroinflammatory microglia observed in various neuron disease situations, including epilepsy (Morin-Brureau *et al.*, 2018), we next evaluated the neuroinflammatory profile in the brain of  $scn1Lab-KD$  larvae. First, we used qRT-PCR to quantify the accumulation in the brain of transcripts encoding two key pro-inflammatory cytokines, interleukin-1 $\beta$  (Il1 $\beta$ ) and interleukin-8 (Il8), and three anti-inflammatory cytokines, interleukin-10 (Il10), interleukin-4 (Il4) and transforming growth factor  $\beta$ -3 (Tgf $\beta$ 3). Surprisingly, we observed no significant changes, neither in the expression of pro-inflammatory markers: *il1 $\beta$*  (WT:  $1.00 \pm 0.22$  vs  $scn1Lab-KD$ :  $1.33 \pm 0.18$ ;  $p > 0.05$ ) and *il8* (WT:  $1.00 \pm 0.09$  vs  $scn1Lab-KD$ :  $0.93 \pm 0.11$ ;  $p > 0.05$ ) (Figure 3A), nor in that of anti-inflammatory markers: *il10* (WT:  $1.00 \pm 0.21$  vs  $scn1Lab-KD$ :  $0.767 \pm 0.17$ ;  $p > 0.05$ ), *il4* (WT:  $1.00 \pm 0.12$  vs  $scn1Lab-KD$ :  $0.89 \pm 0.19$ ;  $p > 0.05$ ) and *tgf $\beta$ 3* (WT:  $1.00 \pm 0.04$  vs  $scn1Lab-KD$ :  $0.876 \pm 0.08$ ;  $p > 0.05$ ) (Figure 3B). Thus although morphological changes seen in  $scn1Lab-KD$  larvae suggested pro-inflammatory microglial activation, no significant increase in the expression of pro- or anti-inflammatory cytokines could be detected in the brain of these individuals. It may be that in this genetic model of epilepsy, levels of neuroinflammation are lower than those observed in rodent pharmacological models, as also suggested by the relatively small percentage of amoeboid microglia in  $scn1Lab-KD$  individuals (~30%). To analyse more precisely microglial expression of Il1 $\beta$  in this genetic context, we generated  $scn1Lab-KD$  larvae also expressing the  $Tg[mpeg1:mcherryF]$  and  $Tg[il1\beta: GFP]$  transgenes (Nguyen-Chi *et al.*, 2015). The results reveal a

significant increase in the percentage of microglia expressing  $Il1\beta$  (WT:  $14.6 \pm 1.7$  vs *scn1Lab*-KD:  $33.6 \pm 1.7\%$ ;  $p < 0.0001$ ) (**Figure 3C-F**). These results confirm an increase in the number



of activated microglial cells in *scn1Lab*-KD embryos, consistent with the increase in the number of "amoeboid" microglia characterized previously.

**Figure 3 : Study of the inflammatory profile of *scn1Lab* embryos.** **A)** Quantification of the expression of the genes encoding the pro-inflammatory cytokines, *il-1 $\beta$*  and *il-8*, relative to that of the *tpb* gene, in the brain of control and *scn1Lab*-KD larvae, aged 4 dpf. **(B)** Quantification of the expression of the genes encoding the anti-inflammatory cytokines, *il-10*, *il-4* and *tgfb3*, relative to that of the *tpb* gene, in the brain of control and *scn1Lab*-KD larvae aged 4 dpf. **(C-D)** Dorsal view of the periventricular stratum of control **(C)** and *scn1Lab*-KD **(D)** 4 dpf larvae, showing microglial cells **(C1, D1)**, *Il-1 $\beta$*  protein expression **(C2, D2)**, as well as the superposition of the two signals **(C3, D3)**. **(E)** Diagram of the head of a zebrafish larva with the area of interest (the periventricular stratum) framed in red. **(F)** Quantification of the percentage of microglial cells expressing the cytokine *Il-1 $\beta$*  in control larvae (N = 19) and *scn1Lab*-KD (N = 16). Scale: 10  $\mu$ m. N = number of larvae analyzed. All images were acquired using a Leica SP8 confocal microscope, equipped with a 20x/water objective with a numerical aperture of 0.75. All graphs represent mean  $\pm$  wk. The p-values were calculated using a Student's t-test. n.s., not significant; \*\*\*\*,  $p < 0.0001$ .

**Microglia ablation increases neuron excitation in *scn1Lab*-KD larvae**

Both the phenotypic changes and  $Il1\beta$  expression observed in microglia of *scn1Lab*-KD larvae strongly suggest that a small, albeit significant, proportion of microglia, 30% of the cells, approximately, respond to neuronal seizures through M1-type pro-inflammatory activation, thus raising the question of whether this microglial response globally mitigates or worsens subsequent excitability of neuronal networks. As a first attempt to address this question, we generated *scn1Lab*-KD larvae expressing the Tg[*HuC*: GCaMP5G] transgene, a sensitive marker of calcium transients in neurons (Akerboom *et al.*, 2012), and fully devoid of microglia following morpholino-mediated inactivation of the *pU.1* gene, which encodes a factor essential for proper differentiation of macrophages and microglia (Rhodes *et al.*, 2005) (Peri and Nüsslein-Volhard, 2008). As previously described (Peri and Nüsslein-Volhard, 2008b), embryos injected with *PU.1* morpholinos are devoid of microglia in the brain as shown by the absence of L-plastin immunostaining (Figure 4 A3) compared with non-injected embryos (Figure 4 A2). With these tools, we analysed and compared neuronal excitation in WT and *scn1Lab*-KD larvae, devoid, or not, of microglia, using simultaneously calcium imaging and local field potential (LFP) recordings.

As previously shown (Liu and Baraban, 2019) (Brenet *et al.*, 2019), when compared to WT individuals, *scn1Lab*-KD larvae display a markedly increased neuronal activity as indicated by the larger number of seizure-like events revealed by either calcium imaging (WT:  $16.5 \pm 1.0$  vs *scn1Lab*-KD:  $32.2 \pm 1.4$ ,  $p < 0.0001$ ) (Figures 4B, 4D<sub>1</sub>) (Supp. Video 5, 6) and LFP recording (WT:  $4.8 \pm 1.2$  vs *scn1Lab*-KD:  $28.2 \pm 2.4$ ,  $p < 0.0001$ ) (Figures 43C, 4E<sub>1</sub>). More importantly, microglia depletion increased the amplitude of neuronal events in both WT and *scn1Lab*-KD larvae (Figure 4D-E), and exacerbated the number of epileptiform events in *scn1Lab*-KD individuals, suggesting that microglia display neuroprotective activity able to mitigate, at least partially, neuronal hyperexcitation.

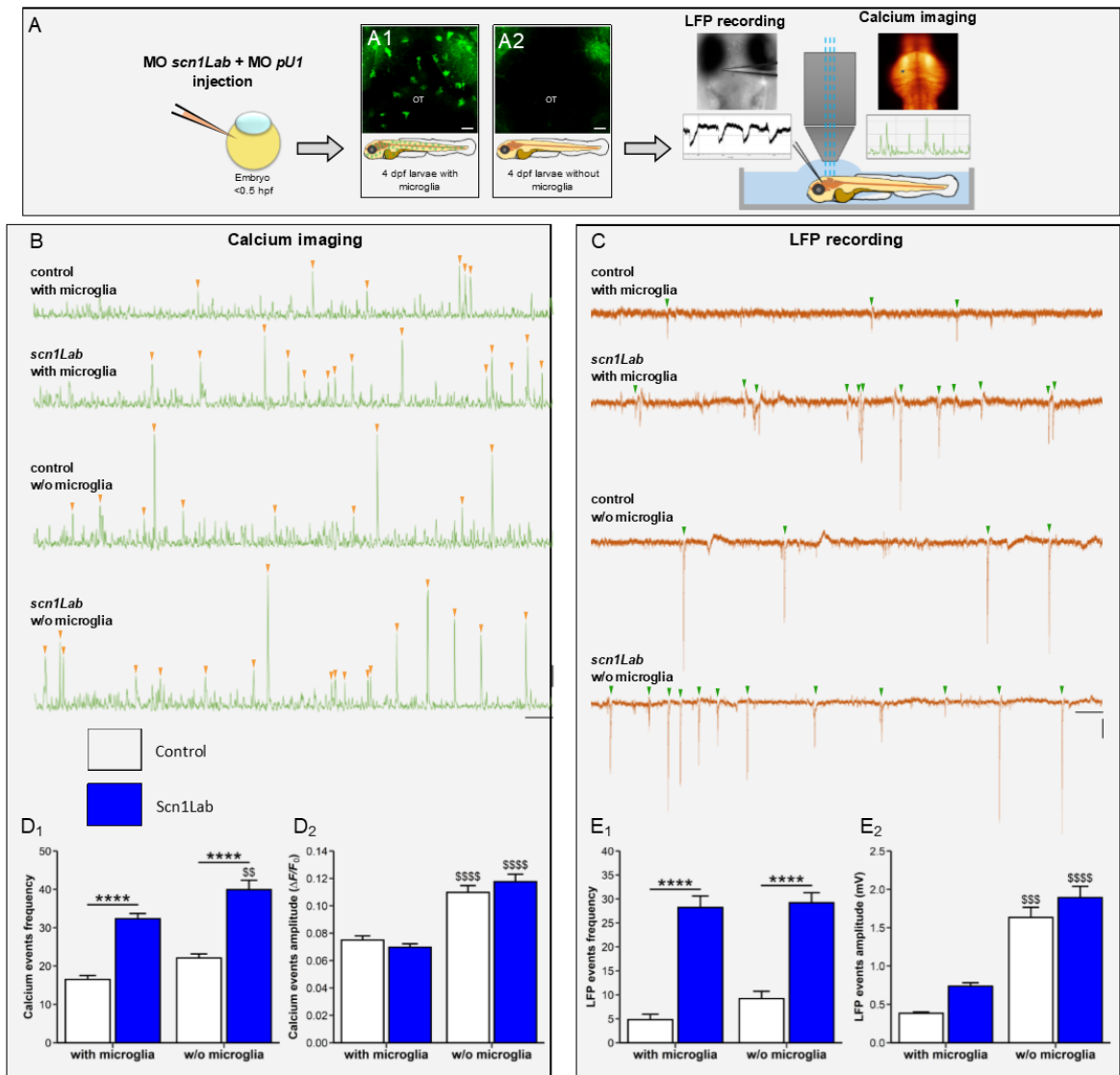


**Figure 4 : Consequences of microglial genetic depletion in the *scn1lab* model.**

(A) Schematic of the experimental set up. (B) 20 min representative calcium traces of 4dpf control ( $N = 11$ ), *scn1Lab* ( $N = 16$ ), control without microglia ( $N = 9$ ) and *scn1Lab* without microglia ( $N = 9$ ) (from top to bottom). (C) 20 min representative LFP traces of 4dpf control ( $N = 5$ ), *scn1Lab* ( $N = 5$ ), control without microglia ( $N = 5$ ) and *scn1Lab* without microglia ( $N = 5$ ) (from top to bottom). Scale bars of calcium traces: 0.05  $\Delta F/F_0$  and 1 min; of LFP traces: 0.5 mV and 1 min. (D) Quantification of calcium events, fluorescence increase greater than 0.04  $\Delta F/F_0$ , frequency (D<sub>1</sub>) and amplitude (D<sub>2</sub>) during 1 hour recording. (E) Quantification of LFP events, downwards depolarization greater than 0.3 mV and lasting more than 100 ms, frequency (E<sub>1</sub>) and amplitude (E<sub>2</sub>) during 1 hour recording. (F) Locomotion tracking plots of 4 dpf control ( $N = 148$ ), *scn1Lab* ( $N = 184$ ), control without microglia ( $N = 45$ ) and *scn1Lab* without microglia ( $N = 288$ ) (from right to left). Larvae velocity is displayed as followed: black represent movements at low speed, green movements at medium speed and red movements at high speed. (G) Quantification of the total distance swum by larvae during 30 min recording.

(H) Quantification of the time spent immobile (H<sub>1</sub>), swimming at low speed (H<sub>2</sub>), swimming at medium speed (H<sub>3</sub>) and swimming at high speed (H<sub>4</sub>). *N* = number of larvae. All data are represented as the mean ± sem. \*\*\*\*, *p* < 0.0001: indicates a statistically significant difference between control and *scn1Lab* larvae. \$\$, *p* < 0.01; \$\$\$, *p* < 0.001; \$\$\$\$ , *p* < 0.0001: indicates a statistically significant difference between larvae with or without microglial cells. *p*-values were determined using two-way ANOVA with Tukey posttests.

### **Microglia ablation exacerbates seizure-like swimming behaviour of *scn1Lab* embryos**

It has been shown that *scn1lab*-KD mutant and morphant exhibit spontaneous seizure-like swimming behaviour consisting of whole-body convulsions and rapid undirected movements (Baraban, Dinday and Hortopan, 2013b) (Brenet *et al.*, 2019). We therefore questioned whether the locomotor activity of *scn1Lab*-KO embryos was dependent on microglia.

Because *scn1Lab*-KD larvae display a distinctive swimming behaviour, characterized by whirling swimming and significantly increased motor activity (Baraban), we next investigated the consequences of the absence of microglia on the locomotor activity of *scn1Lab*-KD embryos (**Figure 5A**). As previously shown, *scn1Lab*-KD larvae swam longer and over longer distances than WT (WT: 212 ± 11 vs *scn1Lab*: 355 ± 11 mm, *p* < 0.0001), reflecting their neuron hyperexcitation (**Figures 5F, 5G, 5H**). Interestingly, in *scn1Lab*-KD larvae devoid of microglia, we observed a markedly increased locomotor activity compared with that observed in *scn1Lab*-KD individuals not microglia-depleted (*scn1Lab*: 355 ± 11 vs microglia-depleted *scn1Lab*: 423 ± 12 mm, *p* < 0.0001) (**Figures 5B-D**), suggesting that microglia depletion worsened the locomotor behaviour of *scn1Lab*-KD larvae and, thus, confirming that neuron excitation was exacerbated in *scn1Lab*-KD larvae lacking microglia compared to that observed in *scn1Lab*-KD individuals.

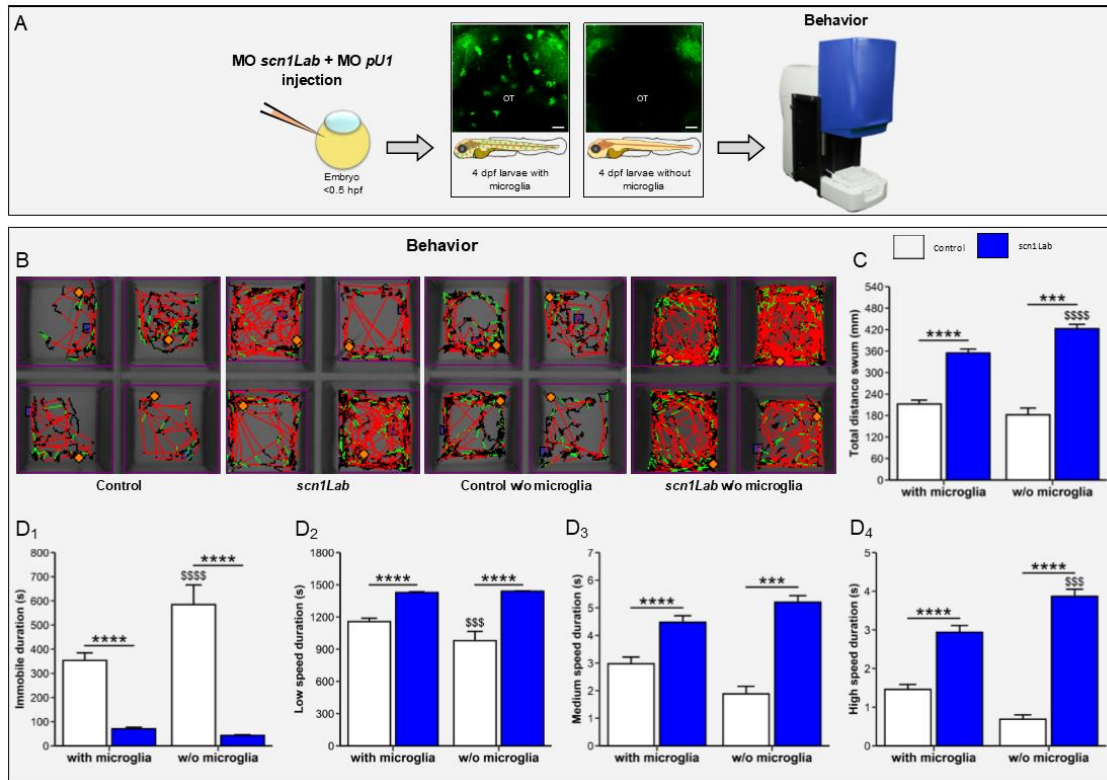


**Figure 5 : Consequences of genetic ablation of microglia on the locomotor activity of *scn1Lab* embryos.** (A) Diagram describing the experimental protocol. (B) Plots of distances traveled by control embryos ( $N = 148$ ), *scn1Lab*-KD ( $N = 184$ ), controls without microglia ( $N = 45$ ) and *scn1Lab*-KD without microglia ( $N = 288$ ) (from right to left). The swimming speed is represented according to the following color code: black represents a low speed, green an intermediate speed and red a high speed. (C) Quantification of the total distance traveled by the embryos during the 30 minutes of recording. (D) Quantification of the time spent by the embryos in a motionless position (D<sub>1</sub>) at low swimming (D<sub>2</sub>) medium (D<sub>3</sub>) high speed (D<sub>4</sub>).  $N =$  number of larvae. All graphs represent the average  $\pm$  sem. The p-values were calculated by a two-way ANOVA followed by a Tukey post-test. \*\*\*,  $p < 0,001$ ; \*\*\*\*,  $p < 0,0001$  : indicates a statistical difference between genotypes. \$\$\$,  $p < 0,001$ ; \$\$\$\$ ,  $p < 0,0001$  : indicate significant differences depending on the presence or absence of microglia.

## Discussion

A close relationship between epileptic seizures and microglia-mediated brain inflammation was established long ago (Vezzani *et al.*, 2004). However, the precise response of microglia to epileptic seizures and its consequences on subsequent neuronal network functioning have so far been scantily studied, especially in *in vivo* models. It has not been known whether seizure-induced microglia activities reduce or exacerbate neuronal network excitability (Lukens and Eyo, 2022). This knowledge gap has several causes, one being that microglia cannot be imaged *in vivo* through the skull in rodents and in most other animal species: transparent windows must be cut, involving delicate surgery and a risk of brain trauma that can influence the state of microglia, which are highly sensitive to disturbances in brain homeostasis (He *et al.*, 2018). Zebrafish larvae offer a useful alternative model because they are transparent, enabling easy imaging of microglial cells in real time and in a living brain in its physiological environment (Peri and Nüsslein-Volhard, 2008c).

Another difficulty has been that most studies investigating microglia activities in rodent epilepsy models have been conducted using pharmacologically-induced neuronal seizures, which cause extended *status epilepticus*-type activity usually lasting several hours (Vezzani, Balosso and Ravizza, 2019a), (Maupu *et al.*, 2021), (Ravizza *et al.*, 2008), (Avignone *et al.*, 2015), and evoke much stronger brain inflammation than that observed in genetic models, and probably human patients (Maupu *et al.*, 2021), (Julie Somkhit, Constantin Yanicostas, 2022), (Somkhit *et al.*, 2022, (Gasmi, 2021). This difficulty can be overcome by using a genetic epilepsy model. We report here what is to our knowledge the first study of the response of microglial cells *in vivo* in such a model.

We chose an established zebrafish model of Dravet syndrome (DS) epilepsy, a severe epileptic encephalopathy caused by a deficit in the activity of inhibitory interneurons, the most common causes of which are *de novo* loss-of-function mutations in the *SCN1A* gene encoding the voltage-gated sodium channel NaV1.1. The zebrafish DS model is based on loss of function of one of the two zebrafish orthologues of the *SCN1A* gene, *scn1lab*, with mutant and morphant *scn1lab* larvae displaying recurrent epileptiform seizures from 3 dpf onward, which we and others had previously characterized (Baraban, Dinday and Hortopan, 2013b) (Brenet *et al.*, 2019). In particular, we previously showed that loss of *scn1lab* function induced a shift in the excitatory/inhibitory balance, with a decrease in the number of GABAergic synapses and an increased number of glutamatergic ones, combined with an increase in the number of apoptotic neurons (Brenet *et al.*, 2019).

In close agreement with findings in both preclinical animal models and human patients (Altmann *et al.*, 2022), microglia displayed major morphological differences in *scn1lab*-KD larvae compared with their wild-type siblings. In the mutant context, we observed a decrease



in the number of ramified microglia and conversely, an increased percentage of microglia showing an amoeboid morphology. These amoeboid microglia probably correspond to the previously described M1-type pro-inflammatory “activated” cells observed after brain injuries or in various neuronal disease situations, including epilepsy (Morin-Brureau *et al.*, 2018), but also following intoxication by neurotoxic compounds, such as organophosphates (Nakajima and Kohsaka, 2001) (Somkhit *et al.*, 2022). Interestingly, although the disease was associated with an increased number of microglia with an “activated” phenotype, the proportion of “transitional” microglia was similar in the two genetic contexts, and a small percentage of “resting” microglia was still observed in *scn1lab*-KD individuals. These observations highlight the complexity of the response of microglia in epilepsy and, more importantly, are evidence that different populations of microglial cells are present in epileptic brains, each likely playing a distinct role in the pathophysiology of the disease. Although increased expression of pro-inflammatory mediators has been observed both in patients with different forms of epilepsy and in various animal models (Morin-Brureau *et al.*, 2018) (Leal *et al.*, 2017), other studies have shown that anti-inflammatory cytokines are also increased in the epileptic brain (Benson, Manzanero and Borges, 2015a), all evidence of a complex response of microglia to epileptic seizures.

Surprisingly, and in contrast with reports in most rodent epilepsy models, qRT-PCR analysis found no significant overexpression of pro-inflammatory cytokine-encoding genes, *il1 $\beta$*  and *il8*, in the brain of *scn1lab*-KD individuals. This result is probably due to the moderate severity of the seizures in these larvae compared with those induced by pharmacological agents, such as PTZ, kainate or DFP (Maupu *et al.*, 2021; Julie Somkhit, Constantin Yanicostas, 2022), whatever the model species. However, using the transgenic Tg[il1 $\beta$ :GFP] line which allows Il1 $\beta$ -expressing cells to be visualized (Nguyen-Chi *et al.*, 2015), we observed a significant increase in the percentage of microglia expressing Il1 $\beta$  in *scn1lab*-KD individuals compared with their WT siblings. This observation, which is in close agreement with our cluster analysis, further confirmed not only the increased number of M1-like “activated” microglia in *scn1lab*-KD larvae, but also the existence of at least two distinct microglia populations, with and without expression of Il1 $\beta$ . However, the increased expression of *il1 $\beta$*  was probably too weak to be detected by qRT-PCR analysis of brain RNAs, highlighting again the differences between genetic and pharmacological epilepsy models (Maupu *et al.*, 2021; Julie Somkhit, Constantin Yanicostas, 2022). It is also of note that studies of microglia-mediated neuroinflammation in *Scn1A*<sup>+/-</sup> mice yielded widely varying results. In some studies, significant activation of microglial cells was observed in the prefrontal cortex and dentate gyrus, combined with an increased expression of the *Il1 $\beta$*  and *Tnfa* genes (Satta *et al.*, 2021), while in other studies, no microglia activation was detected in the hippocampus of *Scn1A*<sup>+/-</sup> mice associated with a lack of over-expression of pro-inflammatory mediators (Salgueiro-Pereira *et al.*, 2019).

Benson et al. (2015) showed that whereas microglia expressed both pro- and anti-inflammatory mediators in the mouse pilocarpine model, only pro-inflammatory mediators were overexpressed in microglia of mice exposed to kainate (Benson, Manzanero and Borges, 2015b). Complex alterations in microglial M1/M2 markers during the development of epilepsy in two mouse models highlighting the wide variety of microglia responses to seizures.

Genetic depletion of microglia in *scn1lab*-KD larvae exacerbated the hyper-excitability of neuron networks as shown by the increased number of spontaneous epileptiform seizures, and worsening of the characteristic swirling swimming behaviour, suggesting that microglia played a protective role in epileptic brains and mitigated neuronal excitability. Like ours, other studies have concluded that microglia play a beneficial role in epilepsy through mitigation of neuronal excitability and modulation of synaptic plasticity (Badimon *et al.*, 2020) (Mirrione *et al.*, 2010; Li, X. F. Du, *et al.*, 2012). In addition, Mirrione et al. (2010) showed that full microglia ablation in adult mice led to an increased sensitivity to the pro-convulsant substance pilocarpine (Mirrione *et al.*, 2010), further evidence that microglia display neuro-protective functions in an epileptic context. However, preventing microglia proliferation using the selective CSF1-R inhibitor GW2580 during the late stage of the epileptogenesis (but not the early stage) decreased spontaneous seizures in the kainate mouse model (Di Nunzio *et al.*, 2021).

This work extends our understanding of the role of microglia in epilepsy. The main added value of our study is that it is the first investigation of the response of microglial cells *in vivo* in a genetic epilepsy model. We show that epileptiform seizures rapidly induce microglia reprogramming characterized by major changes in cell shape and dynamic behaviour, and increased expression of pro-inflammatory cytokine IL-1 $\beta$ . However, this reprogramming is partial and concerns only part of the microglia, suggesting that the response of these cells to seizures is complex and not limited to M1-type activation. Importantly, we also show that *scn1Lab*-KO larvae fully devoid of microglia presented increased numbers of seizures, with greater intensity, suggesting that microglia activity lends neuroprotection to epileptic neurons. Future research will now be needed to investigate the modulation of microglial activities in excitatory neuron protection. Modulating the activities of microglial cells may offer a novel therapeutic strategy of great potential interest in reducing the hyperexcitability of neurons in epilepsies.

## Materials and Methods

### Transgenic lines and fish maintenance

Zebrafish were maintained at 26.5°C in 14 h light and 10 h dark cycles. Embryos were collected by natural spawning and raised at 28.5°C in E3 medium. Developmental stages were determined as hours post-fertilization (hpf) or days post-fertilization (dpf) as previously described (ref). To avoid pigmentation, 0.003% 1-phenyl-2-thiourea (PTU) was added at 1 dpf. The *scn1lab*<sup>s552</sup> line has been previously described (Schoonheim *et al.*, 2010) and was generously provided by the laboratory of Dr. Herwig Baier. Calcium imaging was performed using Tg[*Huc*: GCaMP5G] (Akerboom *et al.*, 2012). Microglia were visualized using Tg[*mpeg1*: mcherryF] (Ellett *et al.*, 2011), and cytokine Il1 $\beta$  expression using Tg[*il1 $\beta$* : GFP] (Nguyen-Chi *et al.*, 2015).

All the animal experiments described were conducted at the French National Institute of Health and Medical Research (INSERM) UMR 1141 in Paris in compliance with European Union guidelines for the handling of laboratory animals ([http://ec.europa.eu/environment/chemicals/lab\\_animals/home\\_en.htm](http://ec.europa.eu/environment/chemicals/lab_animals/home_en.htm)). They were approved by the Direction Départementale de la Protection des Populations de Paris and the French Animal Ethics Committee under reference No. 2012-15/676-0069.

### Morpholino knockdown

The following morpholinos, obtained from Gene Tools, were used in this study: 5'-CTGAGCAGCCATATTGACATCCTGC-3' was used at 0.62 mM to block the *scn1Lab* zebrafish mRNA transcription; 5'-GATATACTGATACTCCATTGGTGGT-3' was used at 0.88 mM to block the *PU.1* zebrafish mRNA transcription. These morpholinos were injected with 0.03 mM rhodamine B dextran and 0.1 mM KCl into stage 1–2 embryos.

### Microglia morphology

4 dpf Tg[*mpeg1*:mcherryF] larvae were paralysed using 300  $\mu$ M parcuronium bromide and agar-immobilized in the centre of a 35 mm glass-bottom dish. A 100  $\mu$ m stack of the larval living optic tectum was acquired at 1024  $\times$  1024 pixel resolution using a Leica SP8 laser scanning confocal microscope equipped with a 20 $\times$ /0.75 multi-immersion objective. Images were processed using AutoQuant 3X (Media cybernetic) and ImageJ software. Surface area, volume and sphericity of microglial cells were quantified using Imaris MeasurementPro (Bitplane). The number and length of microglial processes and their Sholl analysis were determined using Imaris Filament Tracer (Bitplane).

### Clustering of microglial cells

Cluster analysis was performed using the sphericity (S), number of processes (NP), total process length (TL), mean process length (ML), surface area (A) and volume (V) of microglial cells. Microglial cells with at least three of the following features: sphericity less than 0.5, number of processes greater than 7, total process length greater than 140  $\mu\text{m}$ , mean processes length greater than 24  $\mu\text{m}$  and surface area greater than 2400  $\mu\text{m}^2$  were classified as ramified microglia. Conversely, microglial cells with at least three of the following features: sphericity greater than 0.7, number of processes less than 3, total process length less than 60  $\mu\text{m}$ , mean process length less than 17  $\mu\text{m}$  and surface area less than 1500  $\mu\text{m}^2$  were classified as amoeboid microglia. Microglial cells with fewer than three ramified or amoeboid characteristics were classified as transitional microglia.

### **RNA isolation and quantitative RT-PCR**

For RNA isolation, whole larvae or dissected brains were homogenized using a syringe equipped with a 26G needle (7 larvae or 10 brains per sample) using the RNA XS Plus kit (Qiagen, Hilden, Germany). Following RNA quantification with a Nanodrop 2000 (ThermoScientific) and RNA integrity assessment using denaturing gel electrophoresis, total RNAs (1  $\mu\text{g}$ ) were reverse-transcribed into cDNAs using the iScript cDNA Synthesis Kit (Bio-Rad, Germany) and qPCRs were performed using iQ SYBR Green Supermix (Bio-Rad, Germany). Samples were run in triplicate and expression levels of the studied genes were normalized to that of the *tbp* gene. The primers (Eurofins Genomics, Ebersberg, Germany) used are listed in supplementary Table 1.

### **Microglial dynamics**

4 dpf parcuronium bromide-paralysed Tg[mpeg1:mcherryF] larvae were agar-immobilized in the centre of a 35 mm glass-bottom dish. A 42  $\mu\text{m}$  stack of the larval living half optic tectum was acquired at 1024  $\times$  512 pixel resolution every 40 s for 1 h using a Leica SP8 laser scanning confocal microscope equipped with 40 $\times$ /1.1 water objective. Videos were processed using ImageJ software. Microglial cell body displacement, distance travelled between the first and the last frame, and microglial cell body speed displacement were quantified using Imaris MeasurementPro (Bitplane).

### **Calcium imaging**

For quantification, 4 dpf Tg[Huc:GCaMP5G] larvae were paralysed using parcuronium bromide, agar-immobilized in the centre of a recording chamber and placed under a Leica SP8 laser scanning confocal microscope equipped with a 20 $\times$ /0.75 multi-immersion objective. A single focal plane of the optic tectum was captured at a high frequency for 40 minutes. Mean grey value of each frame was measured using ImageJ software and fluorescence variation ( $\Delta F/F_0$ ) was calculated using Excel by subtracting the mean fluorescence intensity of all frames

from the fluorescence intensity of a frame of interest, then normalizing this difference by the mean fluorescence intensity of all frames. The fluorescence drift during recording was corrected by subtracting the background intensity of the surrounding frame. Calcium events were defined as any fluorescence increase greater than  $0.04 \Delta F/F_0$ .

For movie illustration (Supp. Video 5, 6, 7, 8, 13, 14), 5 min calcium recordings of larvae were captured at 5 Hz using a Yokogawa CSU-X1 spinning disk equipped with a 25x/1 multi-immersion objective.

### **Local field potential recording**

Local field potential recording was performed as described in Brenet et al., 2019.

Briefly, 4 dpf larvae were paralysed using parcuronium bromide and agar-immobilized in the centre of a recording chamber. A glass electrode filled with artificial cerebrospinal fluid was placed in the right neuropil of the optic tectum. Neuronal activity was recorded for 1 h in current clamp mode at 10  $\mu$ s sampling interval, amplified with a digital gain of 10, and filtered through a 0.1 Hz high-pass filter and 1 kHz low-pass filter. Recordings were analysed using Clampfit software. Every downward membrane potential variation under  $-0.3$  mV amplitude and lasting more than 100 ms was defined as an event.

### **Locomotor activity**

Larval locomotor activity was assessed using an infrared automated tracking device (ZebraBox), controlled by ZebraLab software. 4 dpf larvae were individually spread in a 96-well plate in 200  $\mu$ L E3 medium. The plate was then placed inside the ZebraBox recording chamber in the dark for 30 minutes habituation after which larvae were tracked for 30 min. Animal colour was set to dark and detection sensitivity to 12 for tracking. Besides the total distance swum by the larvae, we also recorded the number of times that the larvae were immobile, in low-speed movement, medium-speed movement and high-speed movement together with the duration the events. Inactive speed threshold was ??? and high speed threshold was ???. Each experiment replicate comprised at least 16 larvae per condition and completed at least three times.

### **Data analysis**

Data were analysed and plotted using R-studio 1.2.5. Data are presented as mean  $\pm$  sem. Statistical analysis of Figures 1 and 2 was performed using the Mann-Whitney test if data did not follow a normal distribution, otherwise Student's unpaired *t*-test with or without Welch's correction depending on the variance difference. Two-way ANOVA with Tukey post-test was used to analyse data of Figures 3, 4 and 5.

## **Conflict of Interest**

The authors declare that the research was conducted in the absence of any commercial or financial relationships that could be construed as a potential conflict of interest.

**Author Contributions:** AB performed experiments and contributed to the analyses and interpretation of the data. JS performed qRT-PCR. CY co-led the project and contributed to the writing of the article. NSY led the project, designed the experimental research, and contributed to the interpretation of the data and writing of the manuscript. All authors have read and agreed to the published version of the manuscript.

**Funding:** This work was supported by the Institut National de la Santé et de la Recherche Médicale (INSERM), and the National Centre for Scientific Research (CNRS). Funding sources had no involvement in study design, collection, analysis or interpretation of data, nor decision to publish.

**Acknowledgments:** We thank Francesca Peri (University of Zurich, Switzerland) for providing us with the Tg(p2y2:GFP) transgenic line, George Lutfalla (Adresse) for providing us with the Tg(il1 $\beta$ :GFP). We also thank Christiane Romain and Olivier Bar (INSERM UMR 1141) for their technical assistance.

**Conflicts of Interest:** The authors declare no conflict of interest.

## **Supplementary figures:**

**Supplementary-Fig 1A. video 1:** 3D reconstruction of a representative microglia from a control brain's larvae (Fig 1A1). 3D images were generated using Imaris software (Biplane Inc., Version 9.5.0). (link: <https://urlz.fr/iPxZ>).

**Supplementary-Fig 1B. video 2:** 3D reconstruction of a representative microglia from a scn1Lab brain's larvae (Fig. 1B3). 3D images were generated using Imaris software (Biplane Inc., Version 9.5.0). (Link : <https://urlz.fr/iPxP>).

**Supplementary video 3:** Time-lapse of 4 dpf control larvae dorsal view showing microglial displacement and processes dynamic. Interval between frames: 39 s. Video played at x6. Microglial tracking displacement was performed using Imaris software (Biplane Inc., Version 9.5.0). (Link : <https://urlz.fr/iOlz>).

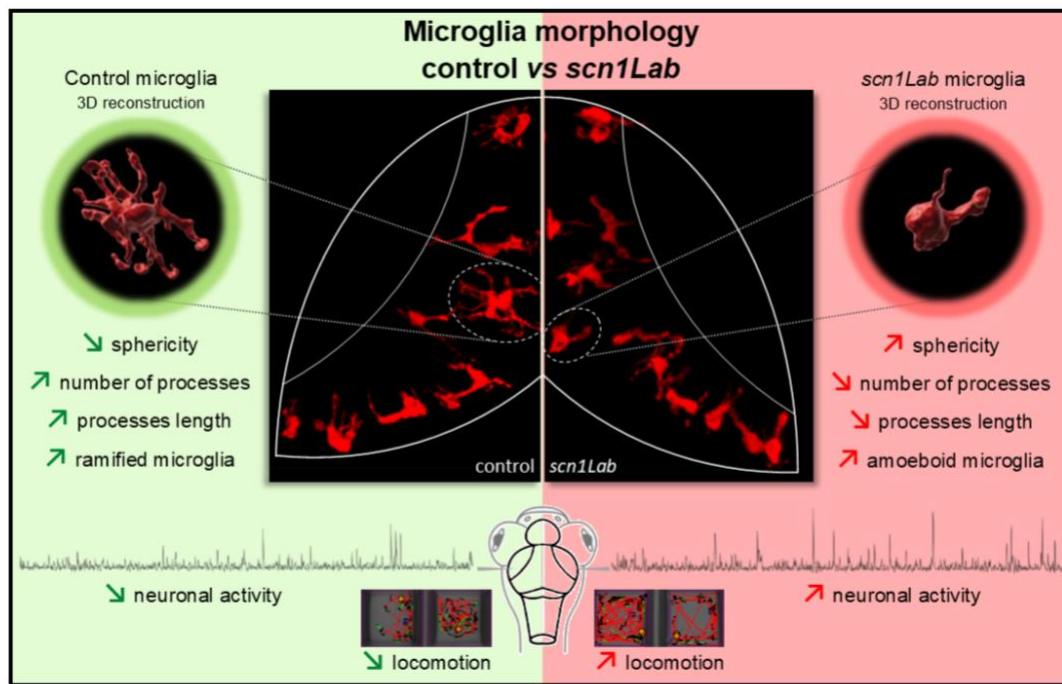
**Supplementary video 4:** Time-lapse of 4 dpf *scn1Lab* larvae dorsal view showing microglial displacement and processes dynamic. Interval between frames: 39 s. Video played at x6. Microglial tracking displacement was performed using Imaris software (Biplane Inc., Version 9.5.0). (Link : <https://urlz.fr/iOIA>).

**Supplementary Figure 2F<sub>1</sub>. Video 5.** Time-lapse of 4 dpf WT larvae dorsal view showing microglial cell body tracking displacement using Imaris software (Biplane Inc., Version 9.5.0). (Link : <https://urlz.fr/iOIC>).

**Supplementary Figure 2F<sub>1</sub>. Video 6.** Time-lapse of 4 dpf *scn1Lab* larvae dorsal view showing microglial cell body tracking displacement using Imaris software (Biplane Inc., Version 9.5.0). (Link : <https://urlz.fr/iOIG>).

#### **Supplenentary table**

<i>il-1β</i>	Forward	5'-CTT AAC CAG CTC TGA AAT GAT G-3'
	Reverse	5'-TGT CGC ATC TGT AGC TCA TTG-3'
<i>il-8</i>	Forward	5'-TGA CCA TCA TTG AAG GAA TGA G-3'
	Reverse	5'-CAT CAA GGT GGC AAT GAT CTC-3'
<i>tnf-α</i>	Forward	5'-TCA CGC TCC ATA AGA CCC AG-3'
	Reverse	5'-GAT GTG CAA AGA CAC CTG GC-3'
<i>il-4</i>	Forward	5'-GAG ACA GGA CAC TAC TCT AAG-3'
	Reverse	5'-GTT TCC AGT CCC GGT ATA TG-3'
<i>il-10</i>	Forward	5'-AAC GAG ATC CTG CAT TTC TAC-3'
	Reverse	5'-CCT CTT GCA TTT CAC CAT AT-3'
<i>tgf-β3</i>	Forward	5'-AAA ACG CCA GCA ACC TGT TC-3'
	Reverse	5'-CCT CAA CGT CCA TCC CTC TG-3'



## Graphical Abstract

## References

- Akerboom, J. *et al.* (2012) 'Optimization of a GCaMP calcium indicator for neural activity imaging', *Journal of Neuroscience*. Society for Neuroscience, 32(40), pp. 13819–13840. doi: 10.1523/JNEUROSCI.2601-12.2012.
- Altmann, A. *et al.* (2022) 'A systems-level analysis highlights microglial activation as a modifying factor in common epilepsies', *Neuropathology and Applied Neurobiology*, 48(1). doi: 10.1111/nan.12758.
- Andoh, M., Ikegaya, Y. and Koyama, R. (2019) 'Synaptic Pruning by Microglia in Epilepsy', *Journal of Clinical Medicine*. MDPI AG, 8(12), p. 2170. doi: 10.3390/jcm8122170.
- Avignone, E. *et al.* (2015) 'Altered morphological dynamics of activated microglia after induction of status epilepticus.', *Journal of neuroinflammation*. Journal of Neuroinflammation, 12(1), p. 202. doi: 10.1186/s12974-015-0421-6.
- Badimon, A. *et al.* (2020) 'Negative feedback control of neuronal activity by microglia', *Nature*. Nature Research, 586(7829), pp. 417–423. doi: 10.1038/s41586-020-2777-8.
- Baraban, S. C., Dinday, M. T. and Hortopan, G. A. (2013a) 'Drug screening in *Scn1a* zebrafish mutant identifies clemizole as a potential Dravet syndrome treatment', *Nature Communications*, 4. doi: 10.1038/ncomms3410.
- Baraban, S. C., Dinday, M. T. and Hortopan, G. A. (2013b) 'Drug screening in *Scn1a* zebrafish mutant identifies clemizole as a potential Dravet syndrome treatment', *Nature Communications*. Nature Publishing Group, 4(1), p. 2410. doi: 10.1038/ncomms3410.
- Benson, M. J., Manzanero, S. and Borges, K. (2015a) 'Complex alterations in microglial M1/M2 markers during the development of epilepsy in two mouse models', *Epilepsia*, 56(6), pp. 895–905. doi: 10.1111/epi.12960.
- Benson, M. J., Manzanero, S. and Borges, K. (2015b) 'Complex alterations in microglial M1/M2



markers during the development of epilepsy in two mouse models', *Epilepsia*. Blackwell Publishing Inc., 56(6), pp. 895–905. doi: 10.1111/epi.12960.

Boer, K. *et al.* (2008) 'Inflammatory processes in cortical tubers and subependymal giant cell tumors of tuberous sclerosis complex', *Epilepsy Research*. Elsevier, 78(1), pp. 7–21. doi: 10.1016/j.epilepsyres.2007.10.002.

Brenet, A. *et al.* (2019) 'Defective Excitatory/Inhibitory Synaptic Balance and Increased Neuron Apoptosis in a Zebrafish Model of Dravet Syndrome', *Cells*. MDPI AG, 8(10), p. 1199. doi: 10.3390/cells8101199.

Carmant, C. E. S. and L. (2015) 'Seizures and Epilepsy : an overview for neuroscientist', *Spring harbor laboratory press*, 1, pp. 5–6. doi: 10.1101/cshperspect.a022426.

Claes, L. *et al.* (2001) 'De Novo Mutations in the Sodium-Channel Gene SCN1A Cause Severe Myoclonic Epilepsy of Infancy', *The American Journal of Human Genetics*. Elsevier, 68(6), pp. 1327–1332. doi: 10.1086/320609.

Dravet, C. (2011) 'Dravet syndrome history', *Developmental Medicine and Child Neurology*. Dev Med Child Neurol, pp. 1–6. doi: 10.1111/j.1469-8749.2011.03964.x.

Ellett, F. *et al.* (2011) 'mpeg1 promoter transgenes direct macrophage-lineage expression in zebrafish', *Blood*. The American Society of Hematology, 117(4), p. e49. doi: 10.1182/blood-2010-10-314120.

Eyo, U. B. *et al.* (2014) 'Neuronal Hyperactivity Recruits Microglial Processes via Neuronal NMDA Receptors and Microglial P2Y12 Receptors after Status Epilepticus', *Journal of Neuroscience*, 34(32), pp. 10528–10540. doi: 10.1523/JNEUROSCI.0416-14.2014.

Fisher, R. S. *et al.* (2014) 'ILAE Official Report: A practical clinical definition of epilepsy', *Epilepsia*. Blackwell Publishing Inc., 55(4), pp. 475–482. doi: 10.1111/epi.12550.

Fisher, R. S. (2015) 'Redefining epilepsy', *Current Opinion in Neurology*, 28(2), pp. 130–135. doi: 10.1097/WCO.0000000000000174.

Gasmi, N. *et al.* (2021) 'Low grade inflammation in the epileptic hippocampus contrasts with explosive inflammation occurring in the acute phase following status epilepticus in rats: translation to patients with epilepsy', *bioRxiv*. Cold Spring Harbor Laboratory, p. 2021.03.25.436701. doi: 10.1101/2021.03.25.436701.

Gasmi, N. *et al.* (2021) 'Low Grade Inflammation in the Epileptic Hippocampus Contrasts with Explosive Inflammation Occurring in the Acute Phase Following Status Epilepticus in Rats', *BioRxiv 2021.03.25.436701*.

Hassan-Abdi, R. *et al.* (2019) 'Neurons Expressing Pathological Tau Protein Trigger Dramatic Changes in Microglial Morphology and Dynamics', *Frontiers in Neuroscience*. Frontiers Media S.A., 13. doi: 10.3389/fnins.2019.01199.

He, Y. *et al.* (2018) 'RNA sequencing analysis reveals quiescent microglia isolation methods from postnatal mouse brains and limitations of BV2 cells', *Journal of Neuroinflammation*, 15(1). doi: 10.1186/s12974-018-1195-4.

Julie Somkhit, Constantin Yanicostas, N. S.-Y. (2022) 'Microglia remodelling and neuroinflammation parallel neuronal hyperactivation following acute organophosphate poisoning', *ijms*.

Kwan, P., Schachter, S. C. and Brodie, M. J. (2011) 'Drug-Resistant Epilepsy', *New England Journal of Medicine*, 365(10), pp. 919–926. doi: 10.1056/NEJMra1004418.

Leal, B. *et al.* (2017) 'Brain expression of inflammatory mediators in Mesial Temporal Lobe Epilepsy patients', *Journal of Neuroimmunology*, 313, pp. 82–88. doi: 10.1016/j.jneuroim.2017.10.014.

Li, Y., Du, X., *et al.* (2012) 'Reciprocal Regulation between Resting Microglial Dynamics and Neuronal Activity In Vivo', *Developmental Cell*, 23(6), pp. 1189–1202. doi: 10.1016/j.devcel.2012.10.027.

Li, Y., Du, X. F., *et al.* (2012) 'Reciprocal Regulation between Resting Microglial Dynamics and Neuronal Activity In Vivo', *Developmental Cell*. Cell Press, 23(6), pp. 1189–1202. doi: 10.1016/j.devcel.2012.10.027.

Liu, J. and Baraban, S. C. (2019) 'Network Properties Revealed during Multi-Scale Calcium Imaging of Seizure Activity in Zebrafish', *eNeuro*. Society for Neuroscience, 6(1), p. ENEURO.0041-19.2019. doi: 10.1523/ENEURO.0041-19.2019.

Lukens, J. R. and Eyo, U. B. (2022) 'Microglia and Neurodevelopmental Disorders', *Annual Review of Neuroscience*, 45(1). doi: 10.1146/annurev-neuro-110920-023056.

Marxer, C. A. *et al.* (2021) 'A review of the evidence on the risk of congenital malformations and neurodevelopmental disorders in association with antiseizure medications during pregnancy', *Expert Opinion on Drug Safety*, 20(12), pp. 1487–1499. doi: 10.1080/14740338.2021.1943355.

Maupu, C. *et al.* (2021) 'Diisopropylfluorophosphate-induced status epilepticus drives complex glial cell phenotypes in adult male mice', *Neurobiology of Disease*, 152. doi: 10.1016/j.nbd.2021.105276.

Mildner, A. (2017) 'Ghosts in the shell: identification of microglia in the human central nervous system by P2Y<sub>12</sub> receptor.', *Neural regeneration research*, 12(4), pp. 570–571. doi: 10.4103/1673-5374.205090.

Mirrione, M. M. *et al.* (2010) 'Microglial ablation and lipopolysaccharide preconditioning affects pilocarpine-induced seizures in mice', *Neurobiology of Disease*. Neurobiol Dis, 39(1), pp. 85–97. doi: 10.1016/j.nbd.2010.04.001.

Morin-Brureau, M. *et al.* (2018) 'Microglial phenotypes in the human epileptic temporal lobe', *Brain*, 141, pp. 3343–3360. doi: 10.1016/0038-1098(79)91043-3.

Nakajima, K. and Kohsaka, S. (2001) 'Microglia: Activation and Their Significance in the Central Nervous System', *Journal of Biochemistry*. Oxford University Press, 130(2), pp. 169–175. doi: 10.1093/oxfordjournals.jbchem.a002969.

Nguyen-Chi, M. *et al.* (2015) 'Identification of polarized macrophage subsets in zebrafish', *eLife*. eLife Sciences Publications Ltd, 4(JULY 2015). doi: 10.7554/eLife.07288.

Di Nunzio, M. *et al.* (2021) 'Microglia proliferation plays distinct roles in acquired epilepsy depending on disease stages', *Epilepsia*, 62(8), pp. 1931–1945. doi: 10.1111/epi.16956.

Peri, F. and Nüsslein-Volhard, C. (2008a) 'Live Imaging of Neuronal Degradation by Microglia Reveals a Role for v0-ATPase a1 in Phagosomal Fusion In Vivo', *Cell*. doi: 10.1016/j.cell.2008.04.037.

Peri, F. and Nüsslein-Volhard, C. (2008b) 'Live Imaging of Neuronal Degradation by Microglia Reveals a Role for v0-ATPase a1 in Phagosomal Fusion In Vivo', *Cell*. Elsevier B.V., 133(5), pp. 916–927. doi: 10.1016/j.cell.2008.04.037.

Peri, F. and Nüsslein-Volhard, C. (2008c) 'Live Imaging of Neuronal Degradation by Microglia Reveals a Role for v0-ATPase a1 in Phagosomal Fusion In Vivo', *Cell*, 133(5), pp. 916–927. doi: 10.1016/j.cell.2008.04.037.

Rana, A. and Musto, A. E. (2018) 'The role of inflammation in the development of epilepsy', *Journal of Neuroinflammation*. BioMed Central Ltd. doi: 10.1186/s12974-018-1192-7.

Ravizza, T. *et al.* (2008) 'Innate and adaptive immunity during epileptogenesis and spontaneous seizures: Evidence from experimental models and human temporal lobe epilepsy', *Neurobiology of Disease*. Academic Press, 29(1), pp. 142–160. doi: 10.1016/j.nbd.2007.08.012.

Rhodes, J. *et al.* (2005) 'Interplay of pu.1 and Gata1 determines myelo-erythroid progenitor cell fate in zebrafish', *Developmental Cell*, 8(1), pp. 97–108. doi: 10.1016/j.devcel.2004.11.014.

Salgueiro-Pereira, A. R. *et al.* (2019) 'A two-hit story: Seizures and genetic mutation interaction sets phenotype severity in SCN1A epilepsies', *Neurobiology of Disease*. Academic Press Inc., 125, pp. 31–44. doi: 10.1016/j.nbd.2019.01.006.

Satta, V. *et al.* (2021) 'Neuropathological Characterization of a Dravet Syndrome Knock-In Mouse Model Useful for Investigating Cannabinoid Treatments', *Frontiers in Molecular Neuroscience*. Frontiers Media S.A., 13, p. 602801. doi: 10.3389/fnmol.2020.602801.

Schoonheim, P. J. *et al.* (2010) 'Optogenetic Localization and Genetic Perturbation of Saccade-Generating Neurons in Zebrafish', *Journal of Neuroscience*, 30(20), pp. 7111–7120. doi: 10.1523/JNEUROSCI.5193-09.2010.

Thurman, D. J. *et al.* (2011) 'Standards for epidemiologic studies and surveillance of epilepsy.', *Epilepsia*, 52 Suppl 7, pp. 2–26. doi: 10.1111/j.1528-1167.2011.03121.x.

Travnickova, J. *et al.* (2015) 'Primitive macrophages control HSPC mobilization and definitive haematopoiesis', *Nature Communications*, 6, pp. 1–9. doi: 10.1038/ncomms7227.

- Vezzani, A. *et al.* (1999) 'Interleukin-1 $\beta$  Immunoreactivity and Microglia Are Enhanced in the Rat Hippocampus by Focal Kainate Application: Functional Evidence for Enhancement of Electrographic Seizures', *The Journal of Neuroscience*, 19(12), pp. 5054–5065. doi: 10.1523/JNEUROSCI.19-12-05054.1999.
- Vezzani, A. *et al.* (2004) 'Functional Role of Proinflammatory and Anti-Inflammatory Cytokines in Seizures', in, pp. 123–133. doi: 10.1007/978-1-4757-6376-8\_10.
- Vezzani, A. *et al.* (2008) 'Glia as a source of cytokines: Implications for neuronal excitability and survival', in *Epilepsia*, pp. 24–32. doi: 10.1111/j.1528-1167.2008.01490.x.
- Vezzani, A. (2013) 'Fetal brain inflammation may prime hyperexcitability and behavioral dysfunction later in life', *Annals of Neurology*, 74(1), pp. 1–3. doi: 10.1002/ana.23930.
- Vezzani, A., Balosso, S. and Ravizza, T. (2019a) 'Neuroinflammatory pathways as treatment targets and biomarkers in epilepsy', *Nature Reviews Neurology*. Nature Publishing Group, pp. 459–472. doi: 10.1038/s41582-019-0217-x.
- Vezzani, A., Balosso, S. and Ravizza, T. (2019b) 'Neuroinflammatory pathways as treatment targets and biomarkers in epilepsy', *Nature Reviews Neurology*. Nature Publishing Group, pp. 459–472. doi: 10.1038/s41582-019-0217-x.
- Vinet, J. *et al.* (2012) 'Neuroprotective function for ramified microglia in hippocampal excitotoxicity', *Journal of Neuroinflammation*. BioMed Central, 9. doi: 10.1186/1742-2094-9-27.
- Woodburn, S. C., Bollinger, J. L. and Wohleb, E. S. (2021) 'The semantics of microglia activation: neuroinflammation, homeostasis, and stress', *Journal of Neuroinflammation*, 18(1), p. 258. doi: 10.1186/s12974-021-02309-6.
- World Health Organization (2019) *Epilepsy*. Available at: <https://www.who.int/news-room/fact-sheets/detail/epilepsy> (Accessed: 10 May 2021).
- Xue-Ping, W. *et al.* (2019) 'Risk factors for drug-resistant epilepsy', *Medicine*, 98(30), p. e16402. doi: 10.1097/MD.00000000000016402.
- Zhang, Y. *et al.* (2015) 'Pharmacological Characterization of an Antisense Knockdown Zebrafish Model of Dravet Syndrome: Inhibition of Epileptic Seizures by the Serotonin Agonist Fenfluramine', *PLOS ONE*. Edited by Y. Herculano-Houzel. Public Library of Science, 10(5), p. e0125898. doi: 10.1371/journal.pone.0125898.